FULL PAPER

Resistive Switching of a Quasi-Homogeneous Distribution of Filaments Generated at Heat-Treated TiO_2 (110)-Surfaces

Maciej Rogala, Gustav Bihlmayer, Wolfgang Speier, Zbigniew Klusek, Christian Rodenbücher, and Krzysztof Szot**

Resistive switching of thermally treated rutile single crystals with (110) orientation is studied. A heat treatment procedure is developed that involves reduction and oxidation steps and allows to induce low resistance states in switchable regions at the surface by low-voltage electrical stimulation with the conducting tip of an atomic force microscope. This way, it is possible to electrically imprint quasi-homogeneous switchable regions over several square micrometers. These regions are identified to consist of nanofilaments crossing the surface with a density of around 10^{12} cm^{-2}, much higher in density than observed for single crystals so far. Experimental evidence is given that these nanofilaments are not related to inherent structural imperfections such as dislocations, but may originate from the linear agglomeration of oxygen vacancies as predicted by theory. Ab initio calculations and electrical simulations are performed to analyze the filamentary structures and their network in the effort to explain the observed filamentary switching of heat-treated single-crystalline TiO_2.

1. Introduction

TiO_2 is considered a prototypical transition metal binary oxide for resistive switching,[1–6] of which the crystalline rutile seems to be most suitable for potential device development. It is now well established that resistive switching in TiO_2 is not a material property by itself but is a highly localized phenomenon in the bulk material related to reduction processes and nanofilamentary structures.[7,8] These structures may develop in single crystalline materials along structural imperfections such as extended defects, e.g., dislocations, through an oxygen redistribution in an initializing (electro-)forming step.[1,9] Nanofilaments could also involve the creation of sub-oxides as a consequence of the extensive local modification of the oxygen stoichiometry[8,11] and it may give rise to a strong spatially confined release of oxygen from the material. The latter has been observed as bubbles occurring underneath the electrodes and may even give rise to a delamination of the electrode material.[12] In fact, the "unpredictable locations and irregular structures"[13] of the nanofilaments are considered to be a serious drawback for device development. Therefore, means are sought to circumvent this problem[5] either by, e.g., doping, developing the material properties in such a way as to offer a controlled generation of nanofilaments in predetermined locations or, alternatively, taking the route of deliberate oxide-layer engineering by, for instance, constructing suitable TiO_2/TiO_{2-x} multilayer structures.[14]

In this work, we describe an approach which allows for the generation of a quasi-homogenous switchable region near the surface which can be used for high density data storage by resistive switching processes. The thermal preparation method that we propose leads to the modification of extended defects in the crystal and creation of "new" filamentary structures of high density near the surface which allows for preferential and fully controllable switching. Basing on experimental and theoretical investigations we deeply analyze the nature of such crystal structure transformation and the mechanism responsible for the observed resistive switching processes.

2. Results and Discussion

The basic mechanism of resistive switching in Ti-based oxides is related to the electrically-induced modification of the local oxygen content along filamentary structures and the corresponding modulation of the electronic properties associated with the occupation of the 3*d*-states (valence change) at the neighboring Ti atoms. This can be achieved in different ways, not only by application of an electrical field, as in resistive

Dr. M. Rogala, Dr. G. Bihlmayer,
Dr. C. Rodenbücher, Prof. K. Szot
Peter Grünberg Institut
Forschungszentrum Jülich
52425 Jülich, Germany
E-mail: rogala@uni.lodz.pl; k.szot@fz-juelich.de
Dr. M. Rogala, Prof. Z. Klusek
Faculty of Physics and Applied Informatics
University of Lodz
Pomorska 149/153, 90-236, Lodz, Poland
Dr. G. Bihlmayer
Institute for Advanced Simulations
Forschungszentrum Jülich
52425 Jülich, Germany
Dr. G. Bihlmayer, Dr. W. Speier, Dr. C. Rodenbücher, Prof. K. Szot
JARA – Fundamentals of Future Information Technology
Forschungszentrum Jülich
52425 Jülich, Germany
Prof. K. Szot
Institute of Physics
University of Silesia
40-007 Katowice, Poland

DOI: 10.1002/adfm.201500855

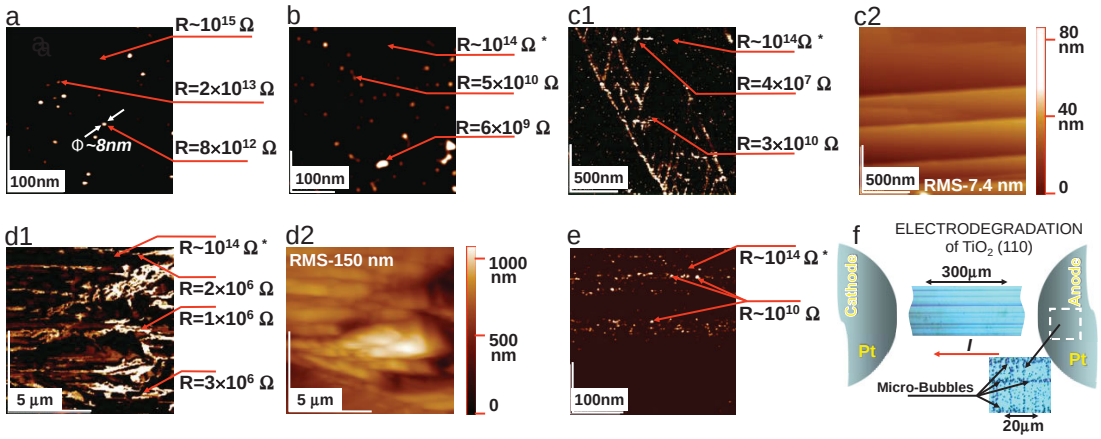

Figure 1. Conductivity (LC-AFM) maps of TiO_2 (110) surface layer obtained by measurements analyzed in more detail in previous paper:[10] a) stoichiometric crystal (sample tip polarization 10 V), b) slightly reduced crystal (polarization 1 V; reduction condition: 800–1000 °C, 1–2 h, ultrahigh vacuum (UHV) conditions: $p_{O2} = 10^{-10}$ mbar, measured by quadrupole mass analyzer), c1) conductivity map (polarization 100 mV) and (c2) topography of strongly reduced crystal (1000 °C; 24 h; UHV), d1) conductivity map (polarization 100 mV) and (d2) topography of heavily reduced crystal (a few days at UHV conditions at 1100 °C or 1 d in a H_2+Ar gas mixture at 1100 °C), e) electro-degraded crystal (polarization 100 mV; temperature below 300 °C), f) a schematic presentation of electrodegradation process. Note that LC-AFM measurements of the resistance of the stoichiometric crystals and for the matrix of the reduced crystals (see resistance values with * indexes) have been obtained using a specially designed *I*/*V* converter with 1 fA sensitivity with sample tip polarization 10 V.

switching, but also by thermal treatment under reducing or oxidizing conditions. As we have recently worked out in detail,[10] one is confronted in all these cases with the fact that the changes induced are indeed highly local in nature and that the modified electrical properties in the bulk material and near the surface exhibit a high level of heterogeneity. This is illustrated in **Figure 1**. Here, we use electrical mapping of the surface employing a local conductivity atomic force microscope (LC-AFM) where the tip of the microscope acts as a point electrode in contact with the surface and measures the current crossing the surface at its position and passing through the crystal to the opposite (e.g., bottom) electrode. Conducting maps of TiO_2 are presented for a reference stoichiometric crystal without any pretreatment (Figure 1a), thermally treated crystals with different level of reduction, here light (Figure 1b), strong (Figure 1c1) to heavy (Figure 1d1) reduction, and an electro-reduced crystal (Figure 1e). LC-AFM maps for stoichiometric and lightly reduced crystals show only a statistical distribution of the filaments. Their conductivity increases as an effect of the removal of oxygen (confirmed via effusion and XPS measurements) in contrast to the resistance of the matrix (in all cases $>10^{14}$ Ω). Although the reduction process changes the electrical properties of the individual filaments, the roughness for stoichiometric and lightly reduced crystals is the same (RMS ≈ 0.2 nm μm^{-2}). A dramatic decrease of the resistance of the filaments has been identified in the LC-AFM maps of the strongly reduced crystal. This thermal treatment is responsible for an additional effect: The filaments are no longer just randomly distributed in the plane of the crystal, a tendency for a linear accumulation of the defects can now be identified. This strong reduction process leads to the modification of the topography (Figure 1c2), which manifests in the increase of the RMS (≈7.4 nm μm^{-2}). The prolonged (heavy) reduction is strong enough to transform surface regions into Magnéli phases, which can be easily identified using X-ray measurements.[8,10] The "electrical consequence" of this extreme reduction is visible in the resistance map (Figure 1d1) and the topography of the surface (Figure 1d2). A very small resistance can be measured in microscopic regions, which have replaced the nanoscopic filament structure or the chains of accumulated filaments seen for strong reduction. A similar effect can be generated using electrical gradients (Figure 1e) but at moderate temperatures (RT-300 °C).[8] A schematic of this so-called electrodegradation is presented in Figure 1f. Prolonged current flow between metal electrodes does not only modify the local transparency (in our case the cathode and anode are connected with a structure of parallel dark stripes), but along the stripe the electrical conductivity is many orders of magnitude higher than in the matrix. On the metal electrode (anode) a high concentration of the micro-bubbles can be identified, which are an indirect proof for the enormous transport of oxygen, which leads to a plastic deformation of the thin metallic electrode at the exits of the stripes. One can see, both in the optical image and the conductivity maps that the filamentary structure has developed between the electrodes in a directed way. The conductivity map further reveals that the optically detectable filaments may actually consist of a bundle of filaments, but all accumulated in stripe-like features in the same direction.

This small gallery of "switched crystals" using both electrical and chemical gradients exemplifies that the homogeneity of the distribution and the density of filaments (or conducting regions) in heat-treated or electro-degraded TiO_2 single crystals has to be considered as being far from what one would consider as being useful for the application as nanodevices for information storage. Also, the overall electrical properties have to be viewed in terms of a mixture of regions in direct spatial proximity, which are characterized by quite diverse electronic

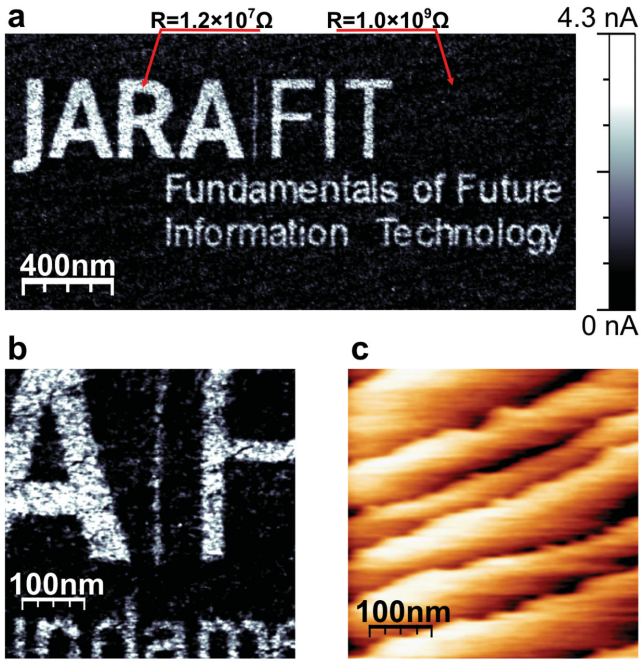

Figure 2. a) LC-AFM conductivity map (sample tip polarization 50 mV) of TiO_2 previously patterned by selectively applying a low voltage (U < 4 V) in the scanned area. b) An enlarged section of the center of the pattern. c) The topographical image corresponding to the area whose conductivity is presented in (b). Before patterning the TiO_2 crystal was prepared by annealing at 1100 °C in UHV and further surface reoxidation by dosing 10^6 L of oxygen at room temperature.

states, either band-insulating in character or in a state where electron correlation plays an important role.

It came as a surprise that, when we tried to test different heat treatment procedures concentrating on low-level reduction in combination with short reoxidation of the surface during in situ experiments, we were able to electrically imprint an astonishingly high concentration of conducting filaments (with a density ≈10^{12} cm^{-2}) with LC-AFM using only low voltages. This is illustrated in **Figure 2**, where a surface of lightly reduced TiO_2 and reoxidation at room temperature is shown which has been selectively electrically addressed with a predetermined pattern. Regions become visible with a quasi-homogenous distribution of high-conducting states at the micrometer scale. These regions are, however, still found to be filamentary in nature. In fact, the logical information is written here in a two-level form, "on" corresponding to high-conducting filaments while "off" corresponding to low-conducting filaments. But, the filaments do not seem to be based on the familiar filaments associated with the structural imperfections such as dislocations, which are not available with this high density and this kind of uniformity at the surface. It is the purpose of the present study to work out the differences in filamentary structures observed at the surface of heat-treated TiO_2 and to obtain further insight into the nature of these "new" filamentary structures. Our analysis was greatly stimulated by the prediction of density functional theory (i.e., ground state) calculations that the agglomeration of oxygen vacancies along linear segments is energetically favorable in the crystalline structure of rutile[15,16] and that linear high-conducting paths may develop and may be easily switchable near the surface during the course of reduction and oxidation, respectively.

For our investigations we used commercial rutile TiO_2 single crystals with (110) orientation obtained by CrysTec, Berlin. In situ measurements with X-ray photoemission spectroscopy (XPS) were performed to monitor changes in electronic character of the crystal as a result of the thermal treatment. The detailed results are shown in the Supporting Information. Our experiments demonstrate that the reduction process does indeed modify the electronic states in the near-surface region through a valence change and is, at least for the lightly reduced crystal, reversible to some extent at room temperature. It is this situation, i.e., light reduction and subsequent reoxidation at room temperature, which was used to electrically address and switch the regions to the high-conducting states presented in Figure 2.

To get further insight into the character of the filamentary structure available at the surface after thermal reduction we investigated the surface of TiO_2 (110) crystals prepared by chemical etching prior to thermal treatment in order to use the etch pits in the standard manner as marks for the position of exits of dislocations (see **Figure 3**a for the topography of an etched surface).[10] Although this preparation step slightly increases the roughness of the surface and generates holes (here the etch pits) at the position where dislocations cross the surface, it does not handicap the redox processes of such chemically modified surfaces. This means that after reduction and reoxidation of an etched crystal it is still possible to electrically address filamentary structures not only at the position of the cores of the dislocations but also at the other places of the surface where no dislocations seem to be available (see Figure 3b), just as noted above. This is even though the crystals were transported through air before being introduced into the LC-AFM chamber. Without electrical activation, the highest conductivity at the surface stems solely from exactly the positions of the etch pits related to the enhanced reduction of the core of dislocations.[10] We have analyzed histograms of selected regions (with the same area 10^4 nm^2) on the described surface of TiO_2 (110) after electrically addressing (as in Figure 3b), one region covering one of the etch pits (area AI in Figure 3a) while the other regions are in close proximity to the etch pit (AII) or further away (AIII). Based on the LC-AFM maps and the study of the histograms (**Figure 4**) for the three mentioned areas we can state are as follows:

1) The distribution of the filaments in the region of the etch pits (the area of AI of 100 nm × 100 nm corresponds approximately to the dimension of the geometrical base of the inverted pyramid of the etch pit) exhibits a sharp maximum with a value of the current of around 30 nA (H_{AI} in Figure 4a). This region AI channels the majority of the current flow through the surface with an integrated current ≈10 μA/10^4 nm^2. In fact, the region is characterized by a dense configuration of filaments within the etch pit and the electrical characteristics of the individual filaments within the area is not strongly marked with the respect to the inner center. Considering the dimensions we might attribute this area not to a single dislocation but rather a highly interwoven bundle of dislocations.

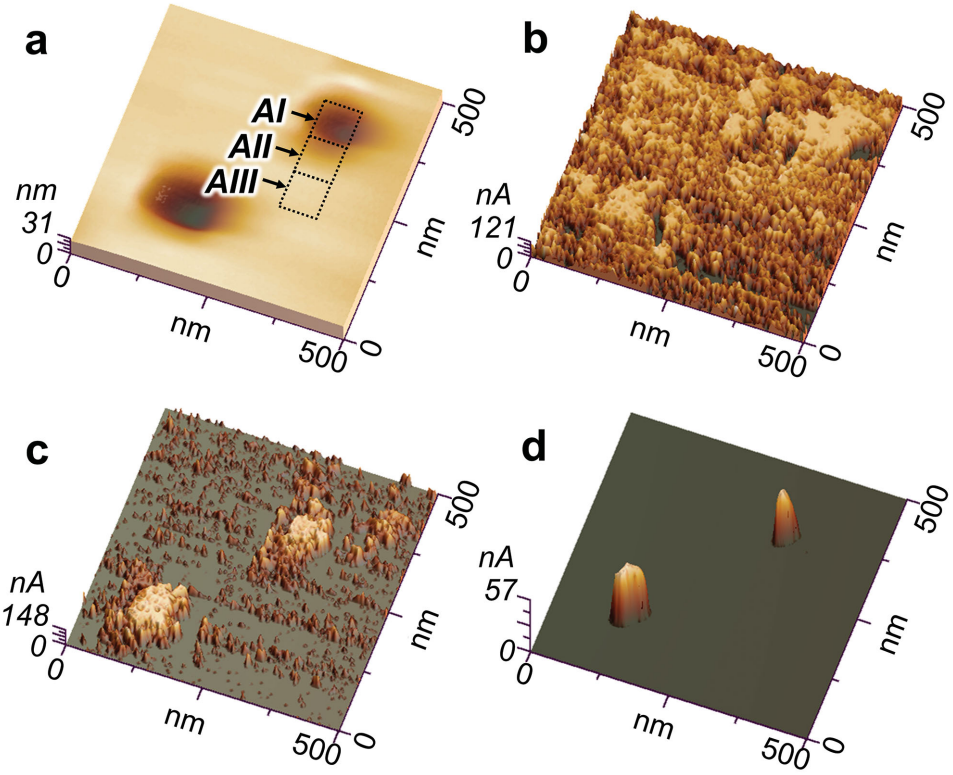

Figure 3. The LC-AFM a) topography and b–d) maps of local conductivity (sample tip polarization 500 mV) of TiO_2 (110) surfaces that have been preliminary etched in HF (etch-pits are visible in topography as inverted pyramid-shaped holes; outside the pits RMS = 0.3 nm). The crystals have been prepared by a multistep technique: (i) slight reduction under UHV conditions and (ii) exposition at RT to oxygen. Low temperature oxidation "switches off" a lion's share of conducting filaments (see dark region in Figure 2a). Electrical gradients (of a few volts via the tip of the LC-AFM) can be using to activate filaments on the nanoscale (b). Here, densities similar to the ones after reduction can be reached. The repeated exposition to controlled doses of oxygen (120 L for (c) and 10^6 L for (d)) "switches off" the electrically activated filaments. However, the filament in the center of etch pit is not sensitive to this oxidation and its conductivity is still high (visible in panel d). Areas, which have been analyzed in the histograms of Figure 4, are indicated in panel (a). More details concerning (a) and (d) can be found in previous paper.[10]

2) The second area (AII) situated in a distance of about 100 nm apart from the center of the etch pit, shows a distinct change in the form of the histogram with respect to the area AI. Instead of a sharp peak, we can identify a broad plateau ranging from 10 to 25 nA (H_{AII} in Figure 4a). The integral current which flows through this region AII, amounting to 0.7μA/10^4 nm^2, is channeled along of individual filaments with typical dimensions of 6–10 nm and is considerably smaller than for the current through the etch pit (i.e., region AI).
3) In the area AIII on the surface we find filaments with a similar radius than for the area AII but the resistance of the individual filaments is higher and their distribution does not show a similarly pronounced plateau as in AII. In the histogram (see H_{AIII} in Figure 4a) we can instead discern a broad

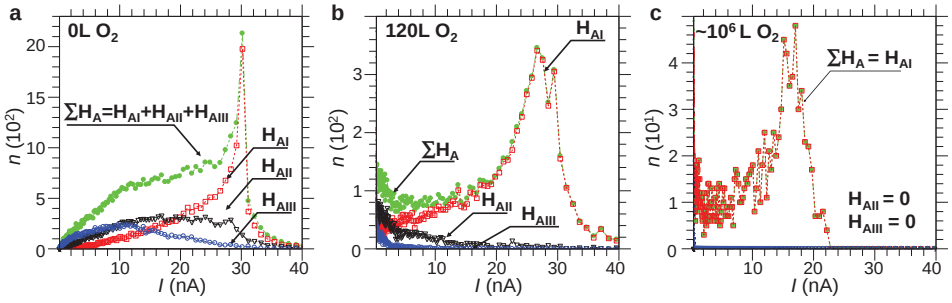

Figure 4. Analysis of the current distribution of the LC-AFM maps presented in Figure 3b–d. The analyses were done for three regions marked in Figure 3a: AI, AII, and AIII, which are "directly at," "close to," and "far from" the etch-pits, respectively. Each region is divided in pixels and the number (n) of pixels with a certain current (I) is shown in the histograms corresponding to various oxygen doses: a) 0L, b) 120L, and c) 10^6 L. Note, that the currents lower than 0.4 nA were cut off to eliminate the measurement noises from analyses.

peak with a "diffuse maximum" centered around 10 nA. The total current flowing through this area AIII (0.4 μA/10^4 nm^2) is 1.7 times smaller than through area AII.

We can conclude on the basis of the histogram analysis that a set of filaments is responsible for the current flow through the surface in the etch pits as well as outside, and that the contribution to the total current decreases with the distance to the etch pit.

Using the same analysis of the histogram for the three chosen areas we also followed the deactivation of the filaments as a function of a reoxidation, here by continuous exposure to an oxygen dose at room temperature. Setting the pressure of oxygen in our vacuum chamber to a value of, in our case, 10^{-4} mbar of p_{O2}, we have obtained, for a dose of oxygen of about 60 L per exposition, a set of the conductivity maps (see, for example, the LC-AFM maps depicted in Figure 3c,d) and individual histograms for the above chosen three areas (collected in Figure 4 corresponding to the electrical maps of Figure 3) as a function of the total oxygen doses (60 L times the number of the oxidation cycles). It becomes immediately obvious that the prolonged exposition has a quite different influence on the individual regions, although the overall tendency is similar in that the integral current for AI, AII, and AIII rapidly decreases (see Table S1 in the Supporting Information).

The histograms for the area AI remain similar for the doses 0 to 180 L, all show a sharp maximum which is shifted from 30 to 28 nA, respectively. The population of the pixels with the value close to the maximum decreases, which means that the radius of the bundle of the filaments in the center of the etch pits becomes gradually smaller. A pronounced change in the position of the maximum of the current from 30 to 18 nA can be identified on the histogram for the area AI for the highest exposition to oxygen in our experiment, here 10^6 L. In this case, the radius of the bundle of filaments in AI has been reduced to 20 nm (compare with LC-AFM map in Figure 3d). In fact, after long time oxidation at slightly elevated temperatures of around 200 °C (not shown) the radius of the filaments can be reduced down to a few nm and a discrete set of the dislocations with ≈2 nm radius per dislocations core can actually be identified.

Turning to the other areas, i.e., outside of the etch pit, the lowering of the electrical conductivity of the filaments in the areas AII and AIII as a function of oxygen exposition shows a much higher dynamics than for the area AI. As can be taken from Table S1, Supporting Information, the decrease in total current through the areas AII and AIII with increasing dose of oxygen (clearly visible in the normalized ratio of the integrated current) is more effective than for the area covering the etch pit. Comparing the dynamics of the deactivation of the electrical "activity" of the areas AII and AIII with respect to the change of the doses from 0 to 180 L one can also draw the conclusion from Table S1, Supporting Information, that the total current through the area AIII, which is further away from the etch pit, decreases more than five times faster than the total current in the direct neighborhood of the etch pit. For the highest oxidation the contribution of both regions, AII and AIII, to the total current can be neglected.

Based on the analysis of LC-AFM maps and histograms, we postulate the existence of two types of filaments, one, which is very sensitive to the exposition of even moderate doses of oxygen and a second type of filaments, which is rather robust against oxidation. In general, the latter filaments, which actually seem to be bundles of filaments, are localized in the center of etch pits. This allows identifying the filaments as conducting cores of dislocations that, in spite of prolonged chemical exposition or electrochemical addressing, remain electrically active. The majority of this "type 1" filaments shows metallic properties. In contrast to the simple classification of the filaments in the middle point of the etch pits as a conducting core of dislocations, the classification of the extended defects that show high sensitivity to oxygen exposure is not as simple.

Density functional theory (DFT) calculations by Park et al.[15] show that conducting line defects along of the certain crystallographic directions in TiO_2 are energetically preferred defect arrangements. These linearly ordered oxygen vacancies are, in our opinion, plausible candidates for the "type 2" filaments which are very sensitive to the oxygen exposition. In contrast to the extended "type 1" filaments, which have to propagate through the crystal until they connect to another defect that keeps the Burgers vector invariant (or, they reach a surface or interface), this type of extended defect can begin or end at any position of the crystal. Therefore, they don't have to form an extended network through the crystal and not necessarily contribute to the total conductivity. The electrical visibility of these segments is then an effect of docking to the network of the conducting "type 1" dislocations.

DFT calculations have already shown that oxygen vacancies in TiO_2 tend to form linear clusters, i.e., rows of missing O atoms. Compared to isolated O vacancies, the formation energy of these linear defects in (110) direction, i.e., normal to the surface plane, is small.[15] The O defects can be created during reduction at the surface, implying, for the growth of the linear defect, that O atoms have to propagate along the defect rows toward the surface. Probably this leads to a large amount of rather short 1D defects extending from the surface down a few nm into the bulk.

The fact, that defects of "type 2" are only electrically active (as seen from the LC-AFM measurements) in a region surrounding the larger "type 1" defects, points to the possibility that they can connect to the network of structurally and electrically more robust "type 1" defect channels that pre-exist in the crystal. This connection can be established, e.g., via 1D oxygen vacancy clusters in (100) direction that show again a small formation energy[15] and can cross a linear defect in (110) direction. The existence of these two types of conducting defects (1 and 2) in a nonconducting matrix is supported by the preferential surface reduction that we observed here (see the XPS description in the Supporting Information) and in our previous X-ray diffraction study (XRD).[8] Other models, e.g., assuming a homogeneously reduced matrix of TiO_2 containing a network of conducting type 2 and 1 defects, where only the latter ones remain conductive under oxidation, are difficult to reconcile with these XRD and XPS data and the presented in situ LC-AFM measurements obtained after the switching of the surface region into "on" state, where an inhomogeneous and filamentary character of material conductivity is observed. Furthermore, in situ measurements of the global resistivity show that the results are changed only slightly after reoxidation of

the reduced crystals in room temperature.[10] This suggests that the electrical conductivity for the samples after our preparation is dominated by the dislocations and the contribution of the homogeneous conductivity is negligible.

In the histograms presented above "type 2" defects appear mainly in region AII, where they contribute to the plateau-like curve that is quickly decreasing with O partial pressure. Assuming that the resistivity decreases linearly with the distance from the large "type 1" defect, the radial arrangement is responsible for the flat shape of the distribution curve. Further away from this defect (area AIII), only occasionally these exits are connected by a 1D channel to the conductive network and the number of filaments decreases with increasing current (see histogram).

To gain an understanding of the conductive properties of different types of defects, we performed DFT calculations of idealized, 1D models: For the model of a "type 1", large-scale defect, we took advantage from the knowledge gained about the stability of TiO_2 nanorods: DFT calculations observed a surprising stability of so-called (2,2)-nanorods that can be seen as part of the rutile structure.[17] In turn, the defect created by removing such a nanorod from the matrix, can be expected to be of similar stability, having a minimal number of broken bonds and being electrically neutral. We simulated this defect using DFT+U calculations as described by Park et al.[18] for a good description of the bulk band gap (2.7 eV). Employing the full-potential linearized augmented planewave method as implemented in the FLEUR code,[19] we calculated a 4×4 unit cell to achieve good separation of the defects in the supercells. The structure was relaxed and is shown (with an additional O defect) in **Figure 5**c.

Comparing the electronic structure of this defect with undefected rutile, our calculations show just a shrinking of the band gap to 2 eV, but no defect states in the gap (not shown). Like in undefected TiO_2, the edge of the valence and conduction band is formed by oxygen and titanium states, respectively. While this neutral defect (we removed four TiO_2 units) is still insulating, removal of an additional O row from the inner surface leads to the formation of a 1D band, as can be seen from Figure 5. This band (easily identified by the two van-Hove singularities in the DOS) appears close to the conduction band edge and the corresponding charge density is shown as a yellow isosurface in Figure 5c. It is easily conceivable that such a reduced defect is electronically conductive, even when the charge state of the defect is changing or additional oxygen atoms are diffusing into this 1D channel (apical oxygen completing one of the TiO_2 octahedra).

Like this large-scale defects, the 1D oxygen defects studied in[15] also provide states to form conductive pathways through the crystal. This could happen when these defects, which can also exist as isolated segments in the bulk, are connected to larger dislocations as described above. We show the electronic structure (DOS) and the charge density of these defect arrangements in (100) and (110) direction in Figure 5a,b. In contrast to the bigger defect discussed above, more or less extended defect states split off the conduction band and reside in the gap. These states are Ti d-electrons located at Ti atoms with two missing oxygen neighbors (i.e., in the center of the defect). This species can be characterized formally as Ti^{2+}, actually Bader charge

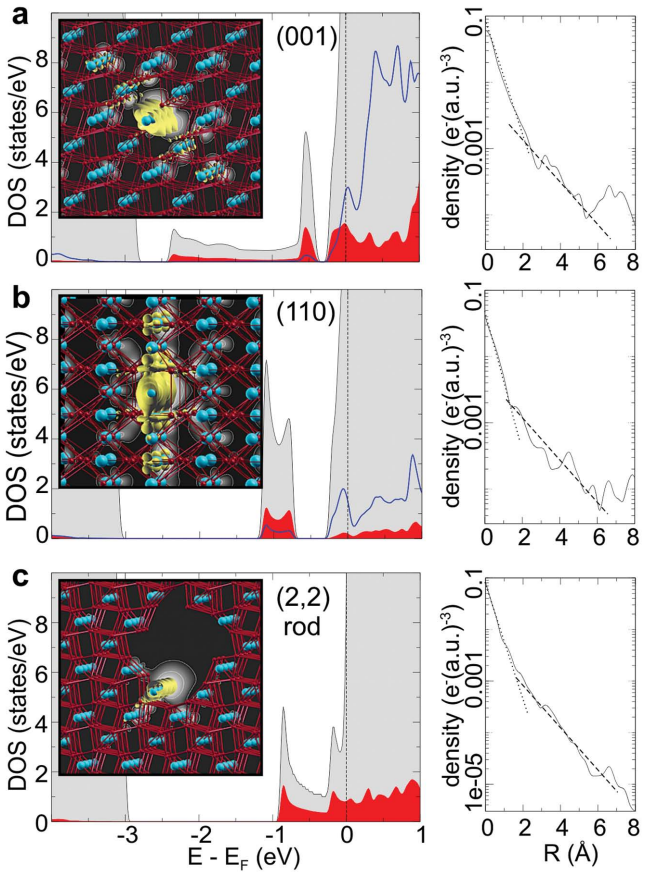

Figure 5. Ab initio simulation of the charge density and electronic structure of three kinds of extended defects in TiO_2: Panels (a) and (b) show rows of oxygen vacancies in (001) and (110) direction, respectively, while panel (c) shows a larger defect with a (2,2)-nanorod removed from the TiO_2 matrix. The inset shows the structure with oxygen atoms in red and Ti atoms in blue. An isosurface (yellow) and a cut through the charge density indicate the extent of the occupied states near the conduction-band edge. A radial integration of this charge density around the defect is shown on the right side of panels. The DOS near the band gap is shown on the left side: The 1D defect states created by the missing row of oxygen appear as split-off state in the gap or at the bottom of the conduction band. The split-off states in panels (a) and (b) are derived from a Ti with two missing O neighbors (red) while the DOS at the bottom of the conduction band is formed by neighboring Ti atoms with only one missing neighbor (blue). In panel (c), this state is mainly derived from the Ti DOS next to the defect (red).

analysis gives a charge around 1.1.[20] These Ti atoms show 2p core-levels shifted by 1.7 eV to lower binding energies (also visible in the XPS data in the Supporting Information). The corresponding charge density is highly localized at the center of the defect and decays quickly as can be seen in the right panels of Figure 5. Besides this very localized Ti d-states, more extended states of neighboring Ti atoms (nominally Ti^{3+} species with 2p core-levels shifted by 0.9 eV or less) are visible at the conduction band edge. They are more extended and contribute to the conductive area around the defect with a diameter of roughly 2 nm.

Despite specific differences, in both directions, (001) and (110), these 1D ordered oxygen vacancies provide metallic

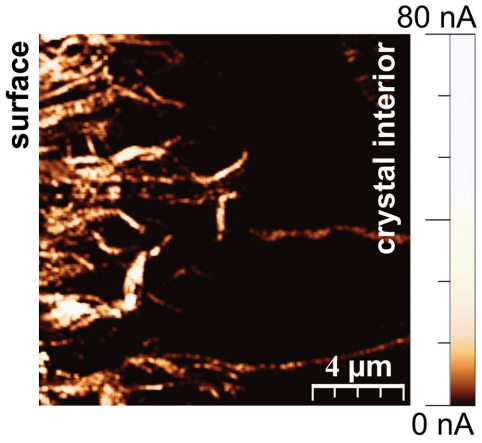

Figure 6. The LC-AFM conductivity map (16 µm × 16 µm, sample tip polarization 700 mV) of the cleavage plane of the near-surface region of previously reduced TiO_2. The left side of the image, where the network of the filaments is most dense, represents the region closest to the surface, while the right part represents the deeper bulk region.

states of similar extensions, which can connect and form an orthogonal conductive network. In contrast to larger defects or defect-bundles, where additional oxygen atoms can be incorporated without affecting the conducting properties, the metallic pathways in these oxygen-vacancy rows are easily disrupted by adding oxygen atoms.[16] Thus, these structures are compatible with the electrically active entities that appear with high density at the TiO_2 surfaces under reducing conditions ("type 2", see above), and that can be switched off with rather small doses of oxygen.

To prove the existence of a hierarchical conducting network of extended defects to which the vacancy rows can connect in the near-surface region, we measured a cross-section generated by cleaving ex situ a reduced crystal (as presented in **Figure 6**). As we find a branched network of dislocations or their bundle is clearly visible in the crystal, exhibiting a particularly high density of branches near the surface. Although this cross-section presents just a planar projection 3D network, the conductivity of the visible segments shows the galvanic connection with the rest of the network that exists in the direction normal to the visible plane. Note, that due to the ex situ preparation the "type 2" defects, which are highly sensible to reoxidation while in contact with air, are not visible in the presented image.

We must consider a number of aspects in order to present a realistic model of the network of both types of extended defects: on the one hand, dislocations with the invariant Burgers vector, "type 1," and, on the other hand, the extended defects named "type 2" above, which are based on 1D ordered oxygen vacancies and which do, however, not have a similar topological invariant as the structural imperfections. The first aspect is the construction of an equivalent circuit of the 3D resistor network, the electrical analysis of which should simulate the kind of hierarchical behavior noted by inspection of the histograms of the conductivity maps of the areas AI, AII, and AIII (see Figure 4). The appropriate simulations were conducted and described in the Supporting Information. For the model electrical circuit that we build the currents in the "on" state show a linear decrease with distance from the center, as observed in the LC-AFM measurements (Table S1, Supporting Information). Simulating the situation after oxygen exposure, i.e., the "off" state, we realized that a good agreement with the experimental data could only be obtained under the assumption that the resistance of the "type 2" defects actually increased with distance from the dislocation core (see annotation of Figure S3 in the Supporting Information). This can be rationalized by the considerations mentioned before, i.e., that the linear arrangements of oxygen vacancies are not only easily created by removal of oxygen, but their conductive properties are more sensitive to the addition of small amounts of oxygen compared to the dislocations. Therefore, the diffusion of oxygen along these defects is decisive in the simulation of the hierarchical network.

For this, we analyzed the oxygen diffusion along a network of "type 2" defects by finite element method as presented in the Supporting Information. The calculated distribution of the oxygen concentration in the crystal correlates to the LC-AFM investigations (compare again with Table S1 in the Supporting Information) in which the filaments of "type 2" furthest away from the "type 1" defect (dislocation) returned to the "off" state upon oxidation much faster than the filaments closer to it.

3. Conclusion

We have seen that the electrical properties of TiO_2 as a result of heat-treatment or electrodegradation (i.e., electroformation) are characterized by large heterogeneities. We would like to stress, as a summary, that despite this fact it seems feasible to obtain switchable regions with a pronounced uniformity, though still filamentary in nature. This has been achieved by combining a light reduction step at elevated temperature with a short reoxidation at room temperature and a subsequent local application of low voltages. We were able to distinguish two types of electrically active filaments crossing the surface with (110) orientation, one type being due to structural imperfections such as dislocations (or dislocation bundles) while the other type of filamentary structure has been generated in the near-surface region 1) with a high density of the order of at least 10^{12} cm^2, being 2) easily oxidisable, and 3) electrically active and switchable by application of low voltages. Based on ab initio calculations (following closely the work of Park et al.)[15] we argue that these filaments are based on extended defects being generated at the surface due to an enforced linear agglomeration of oxygen vacancies along preferential crystallographic directions. Such kinds of extended defects may always form by externally applied reducing conditions, whether as short or long segmental structures. But, in order to become electrically "visible" at the surface through electrical contact (as observed here by LC-AFM), they must develop some kind of network and/or connect to other current transport paths. It is important to stress the fact that such transport paths are indeed available in single crystals in the form of dislocations (or dislocation bundles) due to the fact that such structural imperfections possess a topological invariant, the Burgers vector. Thus, they must extend throughout the crystal, in many cases providing connection of the top surface with the bottom surface, i.e., an electrode positioned at the opposite side. By histogram analysis, we showed a distinctly different behavior of both filamentary structures in that the high-conducting

paths, originating from initially thermally reduced dislocations (peaking in the histogram), are fairly robust against room-temperature oxidation while the other, much smaller filaments (exhibiting a large spread in conductivity) can easily be oxidized (i.e., "switched off") at room temperature. We analyzed the behavior by electrical and diffusion simulations in terms of filaments crossing the surface and interconnected throughout a network in the near-surface region, and being in electrical contact with the filaments of much higher conductivity. Note that our experiments have been undertaken in situ. It is therefore fair to emphasize that the filamentary structure is, on the one hand, easily addressable by the local electrical field, but it is, on the other hand, rather fragile with respect to oxidation. Therefore, any means to extend the long-term stability of such filaments would require a proper encapsulation in order to hinder inward diffusion of oxygen through the surface. As a final conclusion, our observation indicates that the region near the surface offers an easy generation (formation) and switching of nanofilamentary structures which have to be regarded as an inherent feature of the regular crystalline structure of TiO_2 and are well distinguishable from effects related to structural imperfections. Further work is necessary to elucidate the character of this "new" filamentary structure, its network and related properties such as the insulator-metal transition.

Supporting Information

Supporting Information is available from the Wiley Online Library or from the author.

Acknowledgements

The authors acknowledge the financial support by the Deutsche Forschungsgemeinschaft, SFB 917 Nanoswitches and computing time granted at the RWTH Compute Cluster in Aachen. M.R. was supported by the University of Lodz (Grant supporting young scientists).

Received: March 3, 2015
Revised: April 20, 2015
Published online: May 15, 2015

[1] R. Waser, R. Dittmann, G. Staikov, K. Szot, *Adv. Mater.* **2009**, *21*, 2632.
[2] D. S. Jeong, R. Thomas, R. S. Katiyar, J. F. Scott, H. Kohlstedt, A. Petraru, C. S. Hwang, *Rep. Prog. Phys.* **2012**, *75*, 076502.
[3] K. Fröhlich, *Mater. Sci. Semicond. Process.* **2013**, *16*, 1186.
[4] M. Rogala, Z. Klusek, C. Rodenbucher, R. Waser, K. Szot, *Appl. Phys. Lett.* **2013**, *102*, 131604.
[5] D. Acharyya, A. Hazra, P. Bhattacharyya, *Microelectron. Reliab.* **2014**, *54*, 541.
[6] Z. Tang, Y. Chi, L. Fang, R. Liu, X. Yi, *J. Nanosci. Nanotechnol.* **2014**, *14*, 1494.
[7] K. M. Kim, D. S. Jeong, C. S. Hwang, *Nanotechnology* **2011**, *22*, 254002.
[8] K. Szot, M. Rogala, W. Speier, Z. Klusek, A. Besmehn, R. Waser, *Nanotechnology* **2011**, *22*, 254001.
[9] K. Szot, W. Speier, G. Bihlmayer, R. Waser, *Nat. Mater.* **2006**, *5*, 312.
[10] K. Szot, G. Bihlmayer, W. Speier, *Solid State Phys.* **2014**, *65*, 353.
[11] J. P. Strachan, M. D. Pickett, J. J. Yang, S. Aloni, A. L. D. Kilcoyne, G. Medeiros-Ribeiro, R. S. Williams, *Adv. Mater.* **2010**, *22*, 3573.
[12] J. J. Yang, F. Miao, M. D. Pickett, D. A. A. Ohlberg, D. R. Stewart, C. N. Lau, R. S. Williams, *Nanotechnology* **2009**, *20*, 215201.
[13] D. S. Hong, Y. S. Chen, Y. Li, H. W. Yang, L. L. Wei, B. G. Shen, J. R. Sun, *Sci. Rep.* **2014**, *4*, 4058.
[14] J. P. Strachan, J. J. Yang, L. A. Montoro, C. A. Ospina, A. J. Ramirez, A. L. D. Kilcoyne, G. Medeiros-Ribeiro, R. S. Williams, *Beilstein J. Nanotechnol.* **2013**, *4*, 467.
[15] S.-G. Park, B. Magyari-Köpe, Y. Nishi, *IEEE Electron Device Lett.* **2011**, *32*, 197.
[16] B. Magyari-Köpe, S. Park, H.-D. Lee, Y. Nishi, *J. Mater. Sci.* **2012**, *47*, 7498.
[17] D. J. Mowbray, J. I. Martinez, J. M. Garcia Lastra, K. S. Thygesen, K. W. Jacobsen, *J. Phys. Chem. C* **2009**, *113*, 12301.
[18] S.-G. Park, B. Magyari-Köpe, Y. Nishi, *Phys. Rev. B* **2010**, *82*, 115109.
[19] For a program description see: www.flapw.de (accessed: March 2015).
[20] L. Zhao, S.-G. Park, B. Magyari-Köpe, Y. Nishi, *Math. Comput. Modell.* **2013**, *58*, 275.